Analysis of Tilted-Coil Eccentric Borehole Antennas in Cylindrical Multilayered Formations for Well-Logging Applications

Yik-Kiong Hue, *Student Member, IEEE,* and Fernando L. Teixeira, *Senior Member, IEEE*

***Abstract*—Well-logging tools employing tilted coil antennas have been proposed to provide directional (azimuth) information and improved estimates of anisotropy when compared to conventional tools that use horizontal coils. In this paper, we analyze the response of logging tools with tilted coil antennas in eccentric boreholes crossing cylindrical multilayered formations (earth formations with invasion zones) by two approaches. The first approach is based on a pseudoanalytic formulation, previously applied for concentric boreholes and extended here to include eccentric boreholes. The second approach is based on three-dimensional (3-D) numerical simulations using the finite-difference time-domain (FDTD) algorithm extended to cylindrical coordinates and incorporating cylindrical perfectly matched layers (PML). The results from the two formulations are compared for different formations, showing very good agreement.**

***Index Terms*—Finite-difference time-domain (FDTD), logging-while-drilling (LWD), oilfield exploration, tilted-coil antennas.**

I. Introduction

THE analysis of electromagnetic logging tools incorporating transmitter and/or receiver coil antennas that are tilted with respect to the borehole axis is of great interest in applications related to oilfield exploration [1], [2]. In contrast with traditional logging tools that employ horizontal-coil antennas, tilted-coil antennas can provide directional (azimuthal) sensitive data [3], as well as improved estimates of formation anisotropy. For logging-while-drilling/measurement-while-drilling (LWD/MWD) tools, for example, sensitivity to azimuthal orientation around the borehole axis can be employed for improved geo-steering during directional drilling.

Mandrel, borehole, and (piecewise homogeneous) invasion effects in tilted-coil logging tools designs can be characterized using pseudoanalytical formulations. Previous studies have considered cylindrically symmetric borehole problems [4]. Such results show that some configurations are well approximated by (tilted) point dipole antennas, with only minor corrections necessary, but other configurations can depart significantly from the dipole response, especially when invasion effects are considered [4].

Manuscript received March 11, 2005; revised August 8, 2005. This work was supported in part by the NSF under Grant ECS-0347502 and by the OSC under Grants PAS-0061 and PAS-0110.

The authors are with the ElectroScience Laboratory and the Department of Electrical and Computer Engineering, The Ohio State University, Columbus, OH 43212 USA (e-mail: hue.2@osu.edu; teixeira@ece.osu.edu).

Digital Object Identifier 10.1109/TAP.2006.872668

Because of its azimuthal sensitivity, logging tools with tilted coil antennas are attractive for use in deviated or horizontal drilling. However, the tool axis is often eccentric to the borehole axis due to mechanical vibrations and gravitational pull. Therefore, it is important to study the effect of eccentricity [5] on the electrical response (and azimuthal sensitivity) of these tools.

In this paper, we analyze the electrical response of well-logging tools using tilted-coil antenna designs in both cylindrical multilayered and eccentric borehole problems using: i) a three-dimensional (3-D) cylindrical finite-difference time-domain (FDTD) algorithm and ii) a pseudoanalytic formulation for tilted coils [4] augmented here to include eccentric cases [5]. Both approaches can incorporate mandrel effects. The FDTD analysis is computationally more costly, but is able to include more general formation profiles, containing dipping beds and arbitrary invasion zones.

II. Tilted-Coil Well-Logging Tools

Conventional well-logging tools [6]–[9] usually employ horizontal loop antennas. Conventional tools can extract information about the surrounding formation only along the axial (vertical) direction. A tilted-coil LWD/MWD tool consists of tilted antennas that provide directional sensitivity (*azimuthal* information) as well. Unlike a standard tool, a tilted-coil tool not only excites TE_z fields, but also TM_z fields, and can receive both modes. Therefore, it is advantageous over a standard tool when mode coupling occurs, such as in eccentric boreholes. A typical logging tool consists of one tilted transmitter and two tilted receivers around a cylindrical steel mandrel, as illustrated in Fig. 1. Here, we consider coil antennas with radius as measured along the radial direction fixed at 4.5 in. As a result, the larger the tilt angle, the larger is the actual radius of the loops (by a cosine factor). Moreover, the loop antennas assume an elliptic shape, not a circular one, when tilted. The antennas are wrapped around a cylindrical metallic mandrel with 4 in radius. Both angles (elevation and azimuth) of the antennas can be changed, as illustrated in Fig. 2. The center of the transmitter antenna is located at $z = 0$ in. The centers of the first and second receiver antennas are located at $z = 30$ and $z = 24$ in, respectively. The operating frequency is 2 MHz. The parameters of interest are the phase difference (PD) and amplitude ratio (AR) between the voltages at the two receiver antennas.

$$\begin{aligned} \mathrm{PD} &= \theta_{r2} - \theta_{r1} \\ \mathrm{AR} &= \frac{A_{r2}}{A_{r1}} \end{aligned} \tag{1}$$

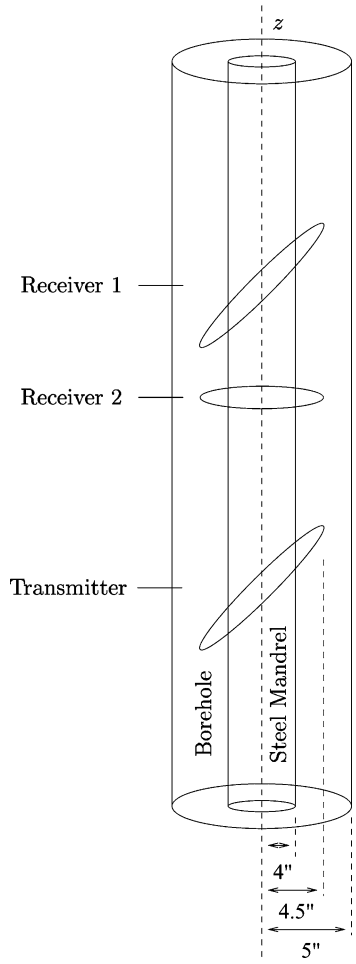

Fig. 1. Tilted-coil LWD tool. The tilting of the transmitter and receivers provides directionality to the tool response.

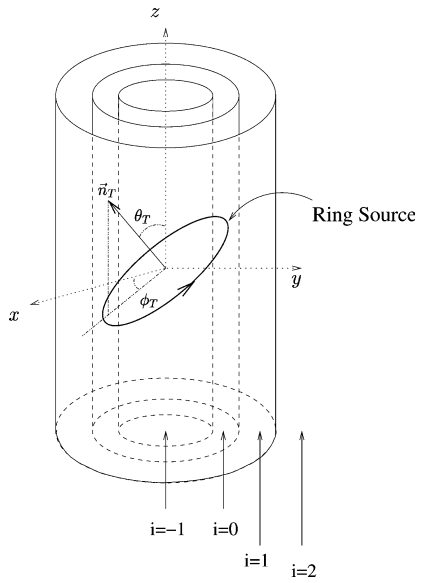

Fig. 2. Tilted coil antenna in a multicylindrical layered medium. The formation is assumed axially symmetric. The source layer is denoted by $i = 0$. Outer layers have positive index, while inner layers have negative index. $\vec{n}_T$ is the normal unit vector to the coil antenna plane.

where θ and A denote phase and magnitude of the voltage at the receivers, and the subscripts $r1$ and $r2$ refer to receivers 1 and 2, respectively.

III. Pseudoanalytic Formulation

An analysis of tilted-coil LWD tools for circularly symmetric formations has been presented in [4] based on the methodology developed in [6]. In this paper, we extend this analysis to tilted coil antennas multicylindrically layered and eccentric formations using the methodology introduced for dipole sources in [5]. We assume a time harmonic excitation of the form $e^{-i\omega t}$.

To solve this problem, the electric and magnetic field are first decomposed into spectral components as

$$\begin{bmatrix} E_z \\ H_z \end{bmatrix} = \frac{1}{2\pi} \sum_{\nu=-\infty}^{+\infty} e^{i\nu\phi} \int_{-\infty}^{+\infty} dk_z e^{ik_z z} \begin{bmatrix} e_{z\nu} \\ h_{z\nu} \end{bmatrix}. \quad (2)$$

In terms of the transformed fields, Maxwell equations reduce to two ordinary differential equations (ODEs) in terms of the radial variable ρ [6], [10], [11]. The general solution for these ODEs are

$$\begin{bmatrix} e_{z\nu} \\ h_{z\nu} \end{bmatrix} = H_\nu^{(1)}(k_\rho\rho)\bar{a}_\nu + J_\nu(k_\rho\rho)\bar{b}_\nu \quad (3)$$

where $H_\nu^{(1)}$ is the Hankel function of first-kind [11], J_ν is the Bessel function, $k_\rho = \sqrt{k^2 - k_z^2}$, $\mathrm{Im}(k_\rho) > 0$ and $k^2 = i\omega\mu(\sigma - i\omega\epsilon)$. The amplitude vectors $\bar{a}_\nu$ and $\bar{b}_\nu$ are 2×1 column vectors to be determined by enforcing appropriate boundary conditions. From (3), the ϕ components of the transformed fields can be obtained as [11]

$$\begin{bmatrix} e_{\phi\nu} \\ h_{\phi\nu} \end{bmatrix} = \bar{\bar{H}}_\nu^{(1)}(k_\rho\rho)\bar{a}_\nu + \bar{\bar{J}}_\nu(k_\rho\rho)\bar{b}_\nu \quad (4)$$

where

$$\bar{\bar{J}}_\nu = \frac{1}{k_\rho^2\rho} \begin{bmatrix} -\nu k_z J_\nu(k_\rho\rho) & -i\omega\mu k_\rho\rho J'_\nu(k_\rho\rho) \\ -(\sigma - i\omega\epsilon)k_\rho\rho J'_\nu(k_\rho\rho) & -\nu k_z J_\nu(k_\rho\rho) \end{bmatrix} \quad (5)$$

and similarly for $\bar{\bar{H}}_\nu^{(1)}$.

To model tilted coil antennas, a ring source is used (see Fig. 2). The source position is given by

$$\vec{r}_T = \hat{\rho}\rho_T - \hat{z}\rho_T \tan\theta_T \cos(\phi - \phi_T). \quad (6)$$

By enforcing boundary conditions along the source location, the following solution for a tilted ring source excitation in a *homogeneous medium* is obtained [4]

$$\begin{bmatrix} e_{z\nu}^h \\ h_{z\nu}^h \end{bmatrix} = \begin{cases} J_\nu(k_\rho\rho)\bar{C}_\nu^- & \rho \le \rho_T \\ H_\nu^{(1)}(k_\rho\rho)\bar{C}_\nu^+ & \rho > \rho_T \end{cases} \quad (7)$$

where

$$\bar{C}_\nu^\pm = \frac{-i\pi}{2} c_{\mathrm{TE}} \begin{bmatrix} \frac{i\omega\mu\nu}{k_z} G_\nu(k_\rho\rho_T) \\ k_\rho\rho_T G'_\nu(k_\rho\rho_T) \end{bmatrix}$$
$$c_{\mathrm{TE}} = i^\nu J_\nu(k_z\rho_T \tan\theta_T) e^{-i(k_z z_T + \nu\phi_T)} \quad (8)$$

where $\bar{C}_\nu^\pm$ are wave amplitudes that satisfy the boundary conditions at the ring source. As shown, G_ν stands for J_ν when the

superscript is $+$ or H_ν when the superscript is $-$. The voltage at the receivers can be determined by a line integral of the electric field along the (loop) receivers positions (see the Appendix).

A. Multicylindrically Layered Medium Case

In this case, we assume a multicylindrically layered formation along the ρ direction, as illustrated in Fig. 2. We still consider a ϕ-invariant formation. The z component of the field in the layer 0 (source layer) can then be expressed as

$$\begin{bmatrix} e_{z\nu} \\ h_{z\nu} \end{bmatrix} = \begin{cases} [H_\nu^{(1)}(k_{\rho_0}\rho)\bar{\bar{M}}_{0\nu} + J_\nu(k_{\rho_0}\rho)\bar{\bar{I}}]\bar{b}_{0\nu} & \rho < \rho_T \\ [H_\nu^{(1)}(k_{\rho_0}\rho)\bar{\bar{I}} + J_\nu(k_{\rho_0}\rho)\bar{\bar{N}}_{0\nu}]\bar{a}_{0\nu} & \rho > \rho_T \end{cases} \tag{9}$$

where $k_{\rho_i} = \sqrt{k_i^2 - k_z^2}$, k_i is the wave number in layer i. $\bar{\bar{M}}_{0\nu}$ and $\bar{\bar{N}}_{0\nu}$ are 2×2 generalized reflection matrices [6]. These two matrices can be derived recursively to incorporate (multiple) reflections from both inner ($i < 0$) and outer ($i > 0$) layers.

The coefficients $\bar{a}_{0\nu}$, the $\bar{b}_{0\nu}$ for a tilted-coil antenna in a multicylindrically layered medium can be obtained by comparing (7) and (9). This leads to the following linear system

$$\begin{pmatrix} \bar{\bar{N}}_{0\nu} & -\bar{\bar{I}} \\ \bar{\bar{I}} & -\bar{\bar{M}}_{0\nu} \end{pmatrix} \begin{pmatrix} \bar{a}_{0\nu} \\ \bar{b}_{0\nu} \end{pmatrix} = \begin{bmatrix} -\bar{C}_\nu^- \\ \bar{C}_\nu^+ \end{bmatrix}. \tag{10}$$

After obtaining $\bar{a}_{0\nu}$, the $\bar{b}_{0\nu}$, the voltage at the receiver for a unit current source at the transmitter (transimpedance) can be calculated as

$$V = \int_0^\infty dk_z \cos[k_z(z_R - z_T)]w(k_z) \tag{11}$$

with

$$w(k_z) = -\rho_R \sum_{\nu=0}^{\infty} \gamma \cos(\nu(\phi_R - \phi_T)) \cdot [d_{\mathrm{TE}}(\nu, k_z)e_{\phi\nu}(\rho_R, k_z) + d_{\mathrm{TM}}(\nu, k_z)e_{z\nu}(\rho_R, k_z)] \tag{12}$$

where

$$\begin{aligned} d_{\mathrm{TE}} &= i^{-\nu} J_\nu(\kappa_R), \\ d_{\mathrm{TM}} &= -\frac{\nu i^{-\nu}}{k_z \rho_R} J_\nu(\kappa_R), \\ \kappa_R &= k_z \rho_R \tan\theta_R \end{aligned} \tag{13}$$

and $\gamma = 1$ if $\nu = 0$ or $\gamma = 2$ otherwise.

B. Eccentric Borehole Case

In practice, due to gravitational pull effects and/or mechanical vibrations, the logging tool axis is often misaligned with the borehole axis. Therefore, analysis of eccentricity effects is important. In this section, we apply the methodology developed in [5] to the case of tilted-coil antennas tools. Fig. 3 illustrates an eccentric tool located d in away from the borehole axis. The segment joining the borehole and mandrel axes makes an angle ϕ_E with the positive x axis. The prime coordinate system is aligned with the mandrel axis, while the unprimed system is aligned with the borehole axis. The z components in the primed system write as

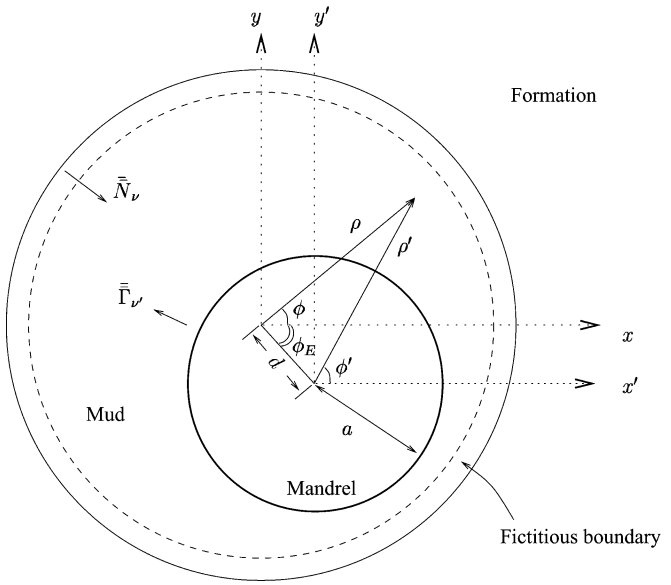

Fig. 3. Illustration of eccentric borehole geometry. The tool (mandrel) axis is located d away from the borehole axis. Nonprimed coordinates are centered on the borehole axis, while primed coordinates are centered on the mandrel axis. The transmitter coil antenna is located inside the borehole (mud filled) region. $\bar{\bar{\Gamma}}_{\nu'}$ is the generalized reflection coefficient due to the mandrel. $\bar{\bar{N}}_\nu$ is the generalized reflection coefficient due to outer formation layers. ϕ'_E is enforced to be zero, and the primed coordinate system is placed at the corresponding location with respect to the unprimed coordinate system.

$$\begin{bmatrix} E_z \\ H_z \end{bmatrix} = \frac{1}{2\pi} \sum_{\nu'=-\infty}^{+\infty} e^{i\nu'\phi'} \int_{-\infty}^{+\infty} dk_z e^{ik_z z} \cdot [H_{\nu'}^{(1)}(k_{\rho'}\rho')\bar{\bar{\Gamma}}_{\nu'} + J_\nu(k_{\rho'}\rho')]\bar{b}_{0\nu'} \quad \rho' \le \rho'_T \tag{14}$$

where $\bar{\bar{\Gamma}}_{\nu'}$ is the reflection matrix at the mandrel given by

$$\bar{\bar{\Gamma}}_{\nu'} = \begin{bmatrix} -\frac{J_{\nu'}(k_\rho a)}{H_{\nu'}^{(1)}(k_\rho a)} & 0 \\ 0 & -\frac{J'_{\nu'}(k_\rho a)}{H'^{(1)}_{\nu'}(k_\rho a)} \end{bmatrix}. \tag{15}$$

In the region $\rho' > \rho'_T$, the solution is given by

$$\begin{bmatrix} E_z \\ H_z \end{bmatrix} = \frac{1}{2\pi} \sum_{\nu'=-\infty}^{+\infty} e^{i\nu'\phi'} \int_{-\infty}^{+\infty} dk_z e^{ik_z z} \cdot \left\{ \left[H_{\nu'}^{(1)}(k_{\rho'}\rho')\bar{\bar{\Gamma}}_{\nu'} + J_{\nu'}(k_{\rho'}\rho') \right] \bar{b}_{0\nu'} + \left[H_{\nu'}^{(1)}(k_{\rho'}\rho')\bar{C}_{\nu'}^+ - J_{\nu'}(k_{\rho'}\rho')\bar{C}_{\nu'}^- \right] \right\} \quad \rho' > \rho'_T \tag{16}$$

where $\bar{C}_{\nu'}^+$ and $\bar{C}_{\nu'}^-$ are determined from the boundary conditions. This expression can be compared with the solution in terms of the nonprimed system.

$$\begin{bmatrix} E_z \\ H_z \end{bmatrix} = \frac{1}{2\pi} \sum_{\nu=-\infty}^{+\infty} e^{i\nu\phi} \int_{-\infty}^{+\infty} dk_z e^{ik_z z} \cdot \left[H_\nu^{(1)}(k_\rho\rho) + J_\nu(k_\rho\rho)\bar{\bar{N}}_{0\nu} \right] \bar{a}_{0\nu} \tag{17}$$

where $\bar{\bar{N}}_{0\nu}$ is the generalized reflection matrix at the borehole wall. Equation (16) and (17) can be matched at the fictitious boundary condition shown by the dashed circle in Fig. 6. To match the two equations, Graf's addition theorem for Bessel functions [12] is used.

$$\Psi_\nu(\nu')e^{i\nu'\phi'} = \sum_{\nu=-\infty}^{\infty} \Psi_\nu(\nu) J_{\nu-\nu'}(d) e^{-i(\nu'-\nu)\phi_E} \tag{18}$$

where Ψ represents a solution of Bessel's equation. Using this identity, the outgoing wave component of (16) can be written as

$$\begin{aligned}
&\sum_{\nu'=-\infty}^{+\infty} e^{i\nu'\phi'} H_{\nu'}^{(1)}(k_{\rho'}\rho') \left[\bar{\bar{\Gamma}}_{\nu'}\bar{b}_{0\nu'} + \bar{C}_{\nu'}^{+}\right] \\
&\quad = \sum_{\nu=-\infty}^{+\infty} e^{i\nu\phi} \cdot H_{\nu}^{(1)}(k_\rho\rho) \sum_{\nu'=-\infty}^{+\infty} J_{\nu-\nu'}(k_\rho d) e^{-i(\nu'-\nu)\phi_E} \\
&\qquad \times \left[\bar{\bar{\Gamma}}_{\nu'}\bar{b}_{0\nu'} + \bar{C}_{\nu'}^{+}\right].
\end{aligned} \tag{19}$$

Similarly, the standing wave component of (16) can be written as

$$\begin{aligned}
&\sum_{\nu'=-\infty}^{+\infty} e^{i\nu'\phi'} J_{\nu'}(k_{\rho'}\rho') \left[\bar{b}_{0\nu'} - \bar{C}_{\nu'}^{-}\right] \\
&\quad = \sum_{\nu=-\infty}^{+\infty} e^{i\nu\phi} \cdot J_\nu(k_\rho\rho) \cdot \sum_{\nu'=-\infty}^{+\infty} J_{\nu-\nu'}(k_\rho d) \\
&\qquad \times e^{-i(\nu'-\nu)\phi_E} \left[\bar{b}_{0\nu'} - \bar{C}_{\nu'}^{-}\right].
\end{aligned} \tag{20}$$

By comparing these two equations with (17), we have

$$\bar{a}_{0\nu} = \sum_{\nu'=-\infty}^{+\infty} J_{\nu-\nu'}(k_\rho d) e^{-i(\nu'-\nu)\phi_E} \left[\bar{\bar{\Gamma}}_{\nu'}\bar{b}_{0\nu'} + \bar{C}_{\nu'}^{+}\right] \tag{21}$$

$$\bar{\bar{N}}_{0\nu}\bar{a}_{0\nu} = \sum_{\nu'=-\infty}^{+\infty} J_{\nu-\nu'}(k_\rho d) e^{-i(\nu'-\nu)\phi_E} \left[\bar{b}_{0\nu'} - \bar{C}_{\nu'}^{-}\right]. \tag{22}$$

Multiplying (21) with $\bar{\bar{N}}_{0\nu}$ and subtracting from (22) gives the following linear system, for all ν.

$$\begin{aligned}
&\sum_{\nu'=-\infty}^{+\infty} J_{\nu-\nu'}(k_\rho d) e^{-i\nu'\phi_E} \left[\bar{\bar{I}} - \bar{\bar{N}}_{0\nu}\bar{\bar{\Gamma}}_{\nu'}\right] \bar{b}_{0\nu'} \\
&\quad = \sum_{\nu'=-\infty}^{+\infty} J_{\nu-\nu'}(k_\rho d) e^{-i\nu'\phi_E} \left[\bar{\bar{N}}_{0\nu}\bar{C}_{\nu'}^{+} + \bar{C}_{\nu'}^{-}\right].
\end{aligned} \tag{23}$$

By solving this linear system, $\bar{b}_{0\nu'}$ can be determined. This gives both $e_{z\nu'}$ and $e_{\phi'\nu'}$. Note that, in numerical calculations, the infinite sum on the azimuthal indexes ν and ν' needs to be truncated. For a given accuracy, the number of modes depends on the borehole size and on the degree of eccentricity. In the results that follow, we use 20 azimuthal modes after ensuring from convergence tests that inclusion of additional modes has negligible effect in the results. The voltage of the receivers can then be computed using (11) with the kernel $w(k_z)$ now given by

$$\begin{aligned}
w(k_z) &= -\rho_R' \sum_{\nu'=-\infty}^{+\infty} e^{i\nu'\phi_R'} \\
&\cdot \left[d_{\mathrm{TE}}(\nu', k_z) e_{\phi'\nu'}(\rho_R', k_z) + d_{\mathrm{TM}}(\nu', k_z) e_{z\nu'}(\rho_R', k_z)\right].
\end{aligned} \tag{24}$$

Note that since the eccentric problem is not invariant along ϕ' anymore, $\bar{b}_{0\nu'}$ has none of the symmetry properties present in the circularly symmetric case. For example, the summation over ν' cannot be folded as done in (12).

IV. FDTD Modeling

The FDTD method [13] can also be extended to analyze this problem [14]–[17]. To avoid staircasing errors in the discretization of the mandrel and antennas geometries along the azimuthal direction, the FDTD is implemented in a 3-D cylindrical grid [17]. To simulate an open-domain problem, an absorbing boundary condition should be used. The 3-D anisotropic-medium cylindrical PML [18] is chosen here for this purpose. In this implementation, the PML is represented by a (cylindrical layered) anisotropic medium inserted at the outer zones of the cylindrical computational domain with permittivity and permeability tensors given by $\bar{\boldsymbol{\epsilon}}_{\mathrm{PML}} = \epsilon\bar{\boldsymbol{\Lambda}}_{[\rho,\phi,z]}(\rho,z;\omega)$ and $\bar{\boldsymbol{\mu}}_{\mathrm{PML}} = \mu\bar{\boldsymbol{\Lambda}}_{[\rho,\phi,z]}(\rho,z;\omega)$ where $\bar{\boldsymbol{\Lambda}}_{[\rho,\phi,z]}(\rho,z;\omega)$ is diagonal tensor (in the cylindrical system) given by

$$\bar{\boldsymbol{\Lambda}}_{[\rho,\phi,z]}(\rho,z;\omega) = \hat{\rho}\hat{\rho}\frac{\tilde{\rho}s_z}{\rho s_\rho} + \hat{\phi}\hat{\phi}\frac{\rho s_z s_\rho}{\tilde{\rho}} + \hat{z}\hat{z}\frac{\tilde{\rho}s_\rho}{\rho s_z} \tag{25}$$

where $\tilde{\rho}$ is the analytic continuation of ρ to a complex domain, and s_ρ, s_z are complex stretching variables defined as

$$s_\rho(\rho) = a_\rho(\rho) + i\frac{\Omega_\rho(\rho)}{\omega} \tag{26}$$

$$s_z(z) = a_z(z) + i\frac{\Omega_z(z)}{\omega} \tag{27}$$

$$\tilde{\rho} = \int_0^\rho s_\rho(\rho')d\rho' = b_\rho(\rho) + i\frac{\triangle_\rho(\rho)}{\omega} \tag{28}$$

where $a_\rho(\rho), a_z(z) \geq 1$ $\Omega_\rho(\rho), \Omega_z(z) \geq 0$. In all FDTD simulation results presented, a cubic profile is used for the stretching variables.

To model eccentric boreholes, a face-based locally conformal FDTD scheme is employed to model the interface between the borehole and formation and minimize staircasing error. In this approach, a weighted average is used to obtain effective conductivities at interface cells. The average is applied to fields normal to the *dual grid faces* where the curved interface intersects. By applying Ampere's equation (in integral form) along dual grid cell faces of the FDTD grid and approximating the electric field as uniform over each dual grid cell face, the effective conductivity σ^{eff} can be written as the weighted average

$$\sigma^{\mathrm{eff}} = \frac{\sigma_1 S_1 + \sigma_2 S_2}{S_1 + S_2} \tag{29}$$

where S_1 and S_2 are the fractional area of the dual grid cell faces corresponding to conductivities σ_1 and σ_2, respectively (e.g., mud and formation conductivities).

To extract frequency data from early time FDTD data and avoid excessive simulation times, we employ an extraction algorithm described in [19]. Nonuniform discretization is adopted along the radial direction of the cylindrical grid, with smaller grid cells used close to the mandrel and larger grid cells used at the outer regions. This allows the simulation of larger domains with less computational cost and without sacrificing geometric modeling accuracy. Further details on these FDTD extensions can be found in [17].

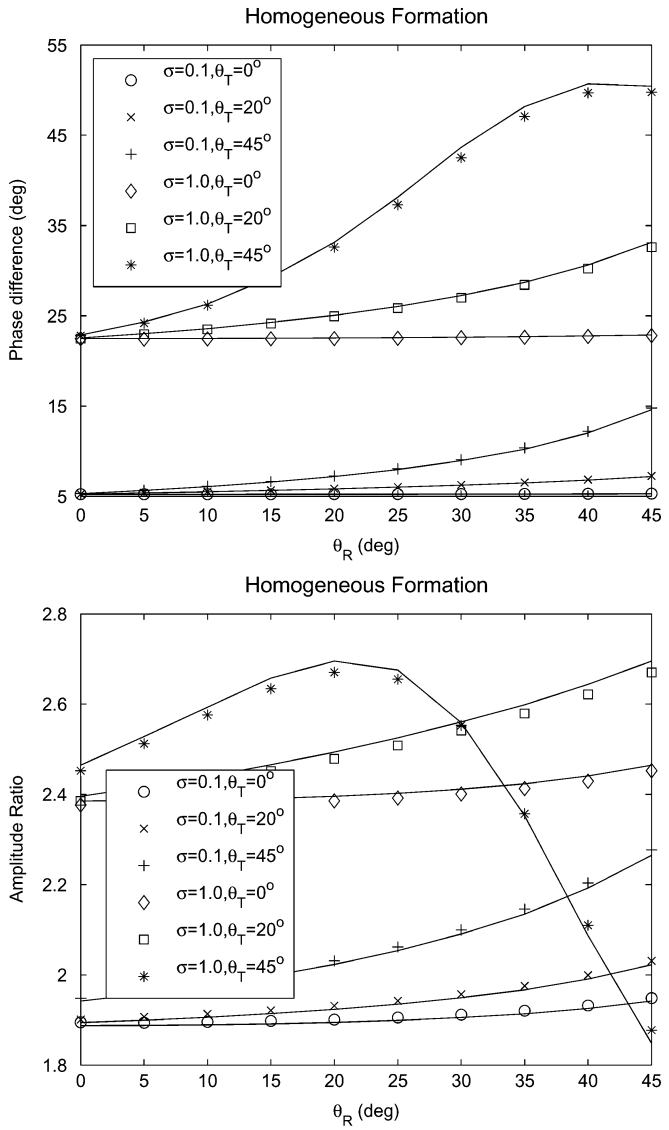

Fig. 4. Comparison between 3-D FDTD and pseudoanalytical results. The tool is located in a homogeneous formation with either $\sigma = 0.1$ mho/m or 1.0 mho/m. Three different tilt angles for the transmitter are considered for each conductivity choice: 0°, 20°, and 45°. Pseudoanalytic results are represent by symbols and FDTD results by solid curves.

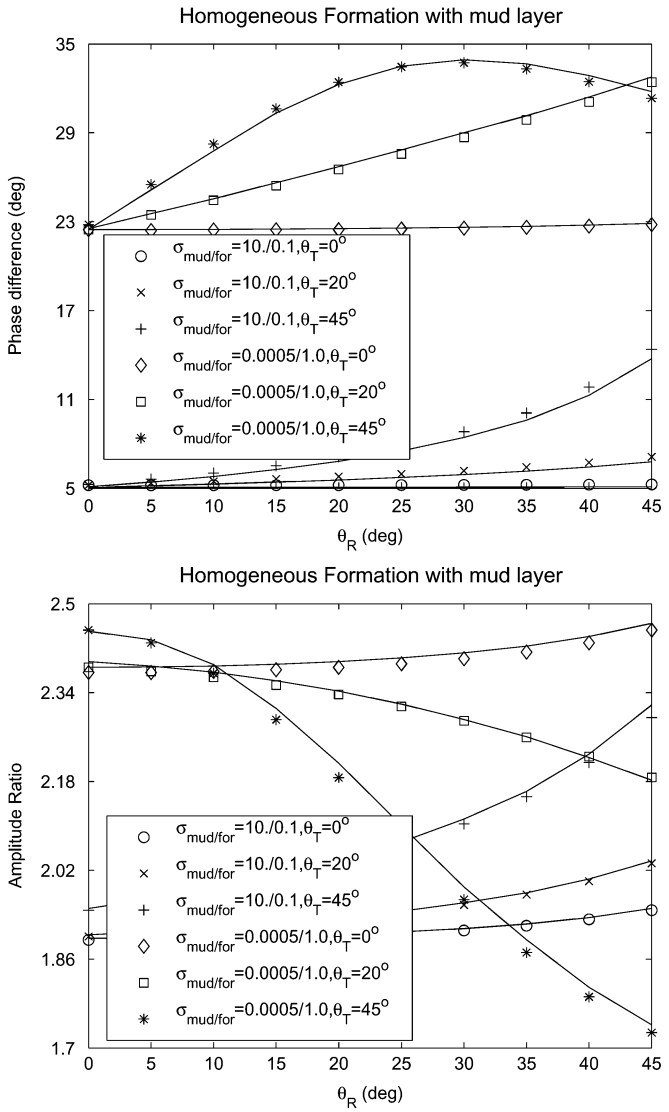

Fig. 5. Comparison between 3-D FDTD and pseudoanalytical results for a tool located in a cylindrical borehole surrounded by a homogeneous formation. Two pairs of borehole mud and formation conductivities are considered: $\sigma_{\mathrm{mud/for}} = 10/0.1$ mho/m and $\sigma_{\mathrm{mud/for}} = 0.0005/1.0$ mho/m. Three different transmitter tilt angles are considered for each pair of conductivities: 0°, 20° and 45°. Pseudoanalytic results represent by symbols and FDTD results by solid lines.

Since the antennas can tilt in both elevation and azimuth angles, the FDTD grid is not fully conformal to the antenna geometry along the z direction. A staircasing approximation along the z direction is currently being used to model the tilted antennas.

V. Results

A. Homogeneous Formations

We first show results for tilted-coil tools in homogeneous formations. We chose two different formation conductivities, $\sigma = 0.1$ mho/m and 1.0 mho/m. For each conductivity value, we simulate three different transmitter tilt angles ($\theta_T = 0°, 20°$, and 45°). The receivers are tilted along the same direction as the transmitter.

Fig. 4 compares 3-D FDTD and pseudoanalytic results. The FDTD solution uses a grid with $(N_\rho, N_\phi, N_z) = (40\,160\,350)$ cells. As mentioned before, the 3-D grid employs nonuniform grid cells in the ρ direction. For $\sigma = 0.1$ mho/m, the radial cell sizes vary from $\Delta\rho = 0.635$ cm close to the mandrel to 18.7670 cm at the outer end. For $\sigma = 1.0$ mho/m, the cell sizes vary from $\Delta\rho 0.635$ cm to 7.11 cm to capture the smaller skin depth. Good agreement is observed between FDTD and pseudoanalytical results.

B. Homogeneous Formations With Mud Layer

We next consider a cylindrical borehole in a homogeneous formation. The conductivity of the borehole mud is assumed uniform. The radius of the borehole is 5 in. Two different cases are considered, one with low mud conductivity and high formation conductivity, and the other with the reverse scenario. For each scenario, we consider three different transmitter tilt angles, equal to 0°, 20° and 45°. The receivers are tilted in the same direction as the transmitter.

Fig. 5 compares 3-D FDTD and pseudoanalytical results. For the FDTD simulation, we use a grid with $(N_\rho, N_\phi, N_z) =$

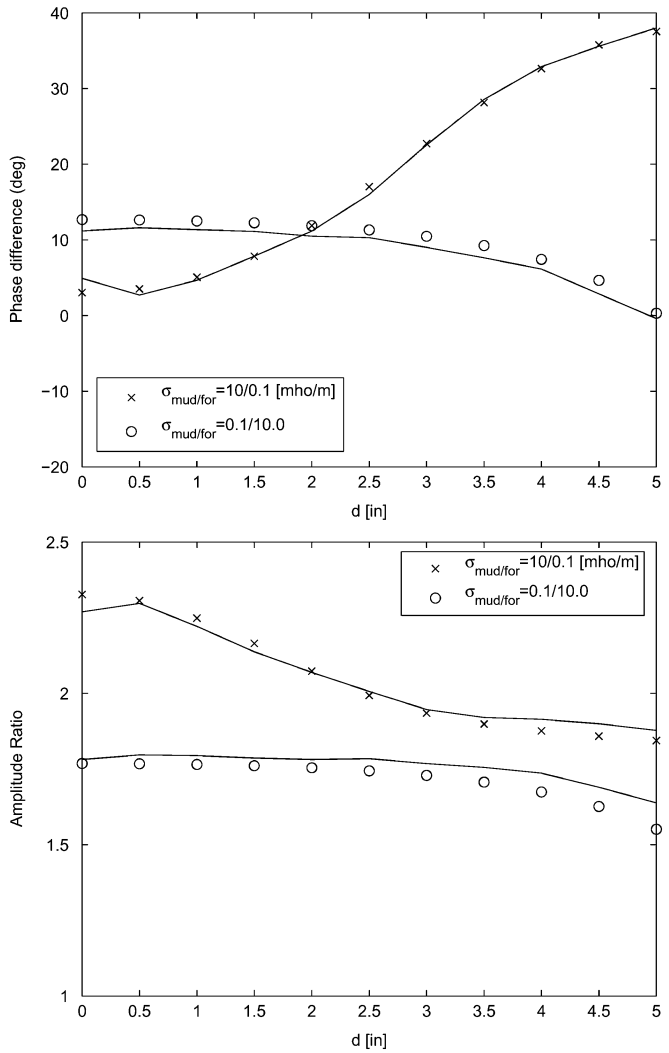

Fig. 6. Comparison between 3-D FDTD and pseudoanalytical results for a tool located in an eccentric cylindrical borehole surrounded by a homogeneous formation. Two pairs of borehole mud and formation conductivities are considered: $\sigma_{\mathrm{mud/for}} = 10/0.1$ and $\sigma_{\mathrm{mud/for}} = 0.1/10.0$ mho/m. The parameter d represents the eccentricity of the tool in inches (see Fig. 3). Both transmitter and receivers have tilt angle equal to 45°. Pseudoanalytical results are represented by symbols and FDTD results by solid curves. See more details in the text.

$(40\,160\,350)$ cells. For the case $\sigma_{\mathrm{mud/for}} = 10.0/0.1$ mho/m, $\Delta\rho$ varies from 0.635 cm to 22.52 cm. For the case $\sigma_{\mathrm{mud/for}} = 0.0005/1.0$ mho/m, $\Delta\rho$ varies from 0.635 cm to 7.11 cm. The comparison between the FDTD results and the pseudoanalytical results shows again very good agreement.

C. Eccentric Boreholes

To better illustrate eccentricity effects, a larger borehole size is chosen in this case, together with a larger conductivity contrast between mud and formation. The radius of the borehole is chosen equal to 12 in. Two formation conductivity cases are considered, as shown in Fig. 3. The transmitter tilted angle equal to 45°. The eccentricity ϕ_E angle is chosen to be $-90°$. The receivers are again tilted in the same direction as the transmitter.

Fig. 6 compares 3-D FDTD and pseudoanalytic results. For $\sigma_{\mathrm{mud/for}} = 10./0.1$ mho/m, we use a FDTD grid with $(N_\rho, N_\phi, N_z) = (40\,160\,350)$ cells and $\Delta\rho$ varying from 0.635 cm to 2.25 cm. For $\sigma_{\mathrm{mud/for}} 0.1/10.0$ mho/m, we use a grid with $(N_\rho, N_\phi, N_z)(40\,200\,350)$ cells and $\Delta\rho$ varying from 0.635 cm to 18.76 cm. Very good agreement is again observed between the two approaches.

VI. Conclusion

We have discusssed the analysis of tilted-coil logging tools in multilayered and eccentric borehole problems using both a pseudoanalytical approach and a brute-force 3-D FDTD numerical scheme. Comparisons between the two approaches for well-logging tools in different borehole and formation scenarios have yielded very good agreement. These two approaches are, in a sense, complementary to each other. In terms of computational requirements, the pseudoanalytical approach is considerably less costly than FDTD modeling. As such, it can be used for a fast turnaround analysis of tool response in simple formations. On the other hand, FDTD is flexible enough to account for highly complex (inhomogeneous) formations, with arbitrary invasion zone profiles, bed boundaries, and dipping bed angles. As such, FDTD can be used to evaluate in more detail the impact of particular formation feature(s) on the response of a given tool. In terms of the main limitations of each approach, the cylindrical FDTD method applied to tilted antennas is restricted by the grid geometry and staircasing approximation. In order to yield good results, the cell size along the z direction need to be fine enough to capture the tilted antenna geometry. For the pseudoanalytical formulation, if the mandrel eccentricity is very large, the linear system given in (34) can become ill-conditioned. In practice, however, this is not expected to occur in usual well-logging tool geometries because borehole and tool radii are not too dissimilar.

This paper has considered boreholes in isotropic formations only. One of the advantages of tilted coil antenna tools is in obtaining improved estimates of anisotropy. The response of tilted coil tools in eccentric borehole through anisotropic formations will be considered in a future work.

Appendix
Pseudoanalytical Formulation: Numerical Considerations

A. Numerical Integration for Multicylindrically Layered Media

The integral in (11) has slow (algebraic) convergence. However, the difference $\tilde{V} = V - V^h$, where V^h is the homogeneous case integral, converges exponentially. V^h can be computed analytically using the radiation integral

$$V^h = -i\omega \frac{\mu \rho_T \rho_R}{4\pi} \int_{-\pi}^{\pi} d\phi' \int_{-\pi}^{\pi} d\phi \bar{u}_T \cdot \bar{u}_R \frac{e^{ikR}}{R} \tag{30}$$

where

$$\bar{u}_T \cdot \bar{u}_R = \cos(\phi - \phi') + \tan\theta_T \tan\theta_R \sin(\phi - \phi_T)\sin(\phi - \phi_R) \tag{31}$$

$$R = \left[\rho_T^2 + \rho_R^2 - 2\rho_T\rho_R\cos(\phi - \phi') + ((z_R - \zeta_R(\phi)) - (z_T - \zeta_T(\phi)))^2\right]^{1/2} \tag{32}$$

and $\zeta(\phi)$ is the position of the antenna in the z-direction. After numerical integration of $\tilde{V}$, V^h can be added to it to obtain V.

B. Condition Number for Eccentric Boreholes

The condition number of the linear system given by (23) can deteriorate for certain ranges of the integrand during the evaluation of the integral in (11) for eccentric cases. This can be circumvented by similarly extracting the homogeneous solution. From (23), $\bar{b}_{0\nu'}$ can in general be decomposed as

$$\bar{b}_{0\nu'} = \bar{C}^{-}_{\nu'} + \bar{\bar{X}}\bar{\Omega}_{\nu'} \tag{33}$$

where the first term corresponds to the homogeneous formation contribution. The second term is the eccentric borehole formation contribution with $\bar{\bar{X}}$ being a free parameter to be optimized. With this decomposition, the linear system in (23) becomes

$$\sum_{\nu'=-\infty}^{+\infty} J_{\nu-\nu'}(k_\rho d)e^{-i\nu'\phi_E}[\bar{\bar{I}} - \bar{\bar{N}}_\nu \bar{\bar{\Gamma}}_{\nu'}]\bar{\bar{X}}\bar{\Omega}_{\nu'} = \sum_{\nu'=\infty}^{+\infty} J_{\nu-\nu'}(k_\rho d)e^{-i\nu'\phi_E}\{\bar{\bar{N}}_\nu[\bar{C}^{+}_0 + \bar{\bar{\Gamma}}_{\nu'}\bar{C}^{-}_0]\} \tag{34}$$

for all ν. The condition number of this system can be modified by choosing an appropriate $\bar{\bar{X}}$. The ϕ' and z components of the field contributed by the eccentric term are given by

$$\begin{aligned}
\tilde{e}_{z\nu'} &= H^{(1)}_{\nu'}(k_\rho\rho'_R)\Gamma^{11}_{\nu'}C^{-\mathrm{TM}}_{\nu'} \\
&\quad + \left[J_{\nu'}(k_\rho\rho'_R) + H^{(1)}_{\nu'}(k_\rho\rho'_R)\Gamma^{11}_{\nu'}\right]x_1\Omega^{\mathrm{TM}}_{\nu'} \\
\tilde{e}_{\phi'\nu'} &= \left[H^{11}_{\nu'}\Gamma^{11}_{\nu'}C^{-\mathrm{TM}}_{\nu'} + H^{12}_{\nu'}\Gamma^{22}_{\nu'}C^{-TE}_{\nu'}\right] \\
&\quad + \left[J^{11}_{\nu'} + H^{11}\Gamma^{11}_{\nu'}\right]x_1\Omega^{\mathrm{TM}}_{\nu'} \\
&\quad + \left[J^{12}_{\nu'} + H^{12}_{\nu'}\Gamma^{22}_{\nu'}\right]x_2\Omega^{\mathrm{TE}}_{\nu'}
\end{aligned} \tag{35}$$

where

$$\begin{aligned}
\bar{\bar{J}}_{\nu'} &= \begin{bmatrix} J^{11}_{\nu'} & J^{12}_{\nu'} \\ J^{21}_{\nu'} & J^{22}_{\nu'} \end{bmatrix}, \quad \bar{\bar{H}}_{\nu'} = \begin{bmatrix} H^{11}_{\nu'} & H^{12}_{\nu'} \\ H^{21}_{\nu'} & H^{22}_{\nu'} \end{bmatrix}, \\
\bar{\bar{\Gamma}}_{\nu'} &= \begin{bmatrix} \Gamma^{11}_{\nu'} & 0 \\ 0 & \Gamma^{22}_{\nu'} \end{bmatrix}, \quad \bar{\bar{X}} = \begin{bmatrix} x_1 & 0 \\ 0 & x_2 \end{bmatrix}, \\
\bar{\Omega}_{\nu'} &= \begin{bmatrix} \Omega^{\mathrm{TM}}_{\nu'} \\ \Omega^{\mathrm{TE}}_{\nu'} \end{bmatrix}
\end{aligned} \tag{36}$$

are given in (5) and (15).

ACKNOWLEDGMENT

The authors thank Dr. L. San Martin of Halliburton Energy Services, Houston, TX, for suggestions and numerous technical discussions.

REFERENCES

[1] M. Bittar, "Electromagnetic wave resistivity tool having a tilted antenna for determining the horizontal and vertical resistivities and relative dip angle in anisotropic earth formations," U.S. Patent 6 163 155, Dec. 19, 2000.

[2] T. Hagiwara and H. Song, "Directional resistivity measurements for azimuthal proximity detection of bed boundaries," U.S. Patent 6 181 138, Jan. 30, 2001.

[3] M. Sato, J. Fuziwara, M. Miyairi, K. Kashihara, and H. Nitsuma, "Directional induction logging methods," in *Proc. SPWLA 35th Ann. Logging Symp.*, Jun. 19–22, 1994, pp. 1–16.

[4] T. Hagiwara, E. J. Banning, R. M. Ostermeier, and S. M. Haugland, "Effects of mandrel, borehole, and invasion for tilt-coil antennas," in *SPE 78th Ann. Tech. Conf. Exhibit.*, Denver, CO, Oct. 5–8, 2003. paper SPE 84 254.

[5] J. R. Lovell and W. C. Chew, "Effect of tool eccentricity on some electrical well-logging tools," *IEEE Trans. Geosci. Remote Sens.*, vol. 28, no. 1, pp. 127–136, Jan. 1990.

[6] ——, "Response of a point source in a multicylindrically layered medium," *IEEE Trans. Geosci. Remote Sens.*, vol. 25, no. 6, pp. 850–858, 1987.

[7] Q. H. Liu, W. C. Chew, M. R. Taherian, and K. A. Safinya, "A modeling study of electromagnetic propagation tool in complicated borehole environments," *The Log Analyst*, vol. 30, pp. 424–436, 1989.

[8] Z. Q. Zhang and Q.-H. Liu, "Simulation of induction logging response using conjugate gradient method with nonuniform fast Fourier and fast Hankel transforms," *Radio Sci.*, vol. 36, no. 4, pp. 599–608, 2001.

[9] F. L. Teixeira and W. C. Chew, "Finite-difference computation of transient electromagnetic waves for cylindrical geometries in complex media," *IEEE Trans. Geosci. Remote Sens.*, vol. 38, no. 4, pp. 1530–1543, Jul. 2000.

[10] J. A. Kong, *Theory of Electromagnetic Waves*. New York: Wiley, 1975.

[11] W. C. Chew, *Waves and Fields in Inhomogeneous Media*. Piscataway, NJ: IEEE, 1995.

[12] *Handbook of Mathematical Functions*, Dover, New York, 1970.

[13] A. Taflove, *Advances in Computational Electrodynamics: The Finite-Difference Time-Domain Method*. Norwood, MA: Artech House, 1998.

[14] T. Wang and G. W. Hohmann, "A finite-difference, time-domain solution for 3-dimensional electromagnetic modeling," *Geophys.*, vol. 58, no. 6, pp. 797–809, 1993.

[15] T. Bergmann, J. O. A. Robertsson, and K. Holliger, "Finite-difference modeling of electromagnetic wave propagation in dispersive and attenuating media," *Geophys.*, vol. 63, no. 3, pp. 856–867, 1998.

[16] S. Wang and F. L. Teixeira, "Dispersion-relation-preserving FDTD algorithms for large-scale three-dimensional problems," *IEEE Trans. Antennas Propag.*, vol. 51, no. 8, pp. 1818–1828, Aug. 2003.

[17] Y.-K. Hue, F. L. Teixeira, L. San Martin, and M. Bittar, "Three dimensional simulation of eccentric LWD tool response in boreholes through dipping formations," *IEEE Trans. Geosci. Remote Sens.*, vol. 43, no. 2, pp. 257–268, Feb. 2005.

[18] F. L. Teixeira and W. C. Chew, "Systematic derivation of anisotropic PML absorbing media in cylindrical and spherical coordinates," *IEEE Microw. Guided Wave Lett.*, vol. 7, no. 11, pp. 371–373, Nov. 1997.

[19] C. M. Furse, "Faster than Fourier: Ultra-efficient time to frequency-domain conversions for FDTD simulations," *IEEE Antennas Propag. Mag.*, vol. 42, no. 6, pp. 24–34, Dec. 2000.

Yik-Kiong Hue (S'01) was born in Kuala Lumpur, Malaysia, on 1977. He received the B.S. and M.S. degrees in electrical engineering from the Ohio State University, Columbus, in 2001 and 2003, respectively.

He joined the ElectroScience Laboratory, Department of Electrical Engineering and Computer Engineering, The Ohio State University, in 2001. He is currently working toward the Ph.D. degree at the Ohio State University. His current research interest includes numerical modeling for geophysical application.

Mr. Hue was the recipient of a 2004–05 SPWLA scholarship.

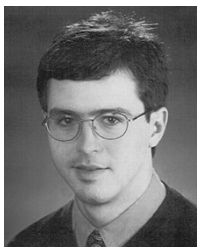

Fernando L. Teixeira (S'89–M'93–SM'05) received the B.S. and M.S. degrees in electrical engineering from the Pontifical Catholic University of Rio de Janeiro (PUC-Rio), Brazil, in 1991 and 1995, respectively, and the Ph.D. degree in electrical engineering from the University of Illinois at Urbana-Champaign, in 1999.

From 1999 to 2000, he was a Postdoctoral Research Associate with the Research Laboratory of Electronics, Massachusetts Institute of Technology (MIT), Cambridge. Since 2000, he has been an Assistant Professor in the ElectroScience Laboratory and the Department of Electrical and Computer Engineering, The Ohio State University, Columbus. His current research interests include analytical and numerical techniques for wave propagation and scattering problems in communication, sensing, and devices applications. He has edited one book *Geometric Methods for Computational Electromagnetics* (Cambridge, MA: PIER 32 EMW, 2001), coauthored more than 60 journal articles and book chapters, and more than 90 conference papers in those areas.

Dr. Teixeira is a Member of Phi Kappa Phi, Sigma Xi, and a Full Member of the International Scientific Radio Union (URSI) Commission B. He was awarded many prizes for his research including the NSF CAREER Award in 2004 and the triennial USNC/URSI Booker Fellowship in 2005.